Available online at www.sciencedirect.com
ScienceDirect
Polymer 47 (2006) 7970–7979
polymer
www.elsevier.com/locate/polymer

Effect of metal nanoparticles on thermal stabilization of polymer/metal nanocomposites prepared by a one-step dry process

Jae-Young Lee [a], Yonggui Liao [a], Ritsuko Nagahata [b], Shin Horiuchi [a,*]

[a] *Nanotechnology Research Institute, National Institute of Advanced Industrial Science and Technology (AIST), 1-1-1 Higashi, Tsukuba, Ibaraki 305-8565, Japan*

[b] *Research Institute for Innovation in Sustainable Chemistry, National Institute of Advanced Industrial Science and Technology (AIST), 1-1-1 Higashi, Tsukuba, Ibaraki 305-8565, Japan*

Received 4 June 2006; received in revised form 18 August 2006; accepted 15 September 2006
Available online 9 October 2006

Abstract

Palladium (Pd) nanoparticles were incorporated into free-standing polymer films by a one-step dry process involving simultaneous vaporization, absorption and reduction schemes of palladium(II) bis(acetylacetonate), $Pd(acac)_2$, used as a precursor. Matrix-assisted laser desorption/ionization time-of-flight mass spectrometry (MALDI-TOF MAS) and Fourier transform infrared spectroscopy (FTIR) analyses showed that the polymers maintained their molecular structures throughout the process. The metal nanoparticles were selectively loaded into the amorphous regions between the lamellae of crystalline polymers having higher melting temperatures than the processing temperature (180 °C). The uniformly dispersed Pd nanoparticles retarded the thermal decomposition of polystyrenes, polypropylene and a methacrylate polymer, and accelerated the thermal decomposition of polyamide 6 and poly(ethylene terephthalate), as seen from the results of thermogravimetric analysis (TGA). Kinetic studies showed that retardation of the degradation was mainly due to suppression of the mobility of polymer chains by the Pd nanoparticles, while acceleration of the degradation was mainly attributed to a decrease in the degradation activation energy due to the catalytic role of the Pd nanoparticles.

Keywords: Metal nanoparticles; Polymer nanocomposite; Thermal degradation

1. Introduction

Nano-sized metals have special characteristics that may allow their use in a number of advanced functional applications. However, their use has been limited by the difficulties associated with handling small objects. They are easily aggregated because of their high surface free energy, and can be oxidized or contaminated in air. Embedding of nano-sized metals into dielectric matrices represents a valid solution to these aggregation and stabilization problems. Polymers are particularly interesting as an embedding medium as they may impart a variety of useful characteristics. The methods for loading of the metal nanoparticles into a polymer can mainly be classified as: (1) a metallic precursor is dissolved along with a polymer in a solvent, and then reduced to the metallic nanoparticles during stirring, heating and evaporating the solvent [1–4]; (2) a metallic precursor is dissolved in a monomer, and then reduced to the metallic nanoparticles during polymerization [5–7]; (3) a colloidal solution of metal nanoparticles, prepared by a pretreatment, is mixed with either a monomer or a polymer solution, followed by a procedure similar to (1) or (2) [8,9]; and (4) a polymer matrix is impregnated with a solvent containing a metal precursor, and then is either treated by reduction agents or subjected to thermolysis [10,11]. Uniformly dispersed metal nanoparticles in a polymer matrix offer strong possibilities of fabricating functional materials with useful catalytic [1,12], optical [2,3,5,13], sensing [14], magnetic [4,15,16], or electrical [17,18] properties. Therefore, many researchers have devoted their work to

* Corresponding author. Tel.: +81 29 861 6281; fax: +81 29 861 4773.
E-mail address: s.horiuchi@aist.go.jp (S. Horiuchi).

0032-3861/$ - see front matter © 2006 Elsevier Ltd. All rights reserved.
doi:10.1016/j.polymer.2006.09.034

the development of new polymer/metal nanocomposites [19]. However, only a few polymers can be used as host matrices using those methods due to many process limitations such as their solubility in the solvents used, ability to polymerize in the presence of a precursor, miscibility of a precursor to a polymer, high glass transition and melting temperatures of host polymers, and so on.

We have previously developed and reported a simple one-step dry process involving simultaneous vaporization, absorption and reduction schemes of palladium(II) bis(acetylacetonate), $Pd(acac)_2$, used as a precursor [20–27]. $Pd(acac)_2$ was vaporized in a nitrogen atmosphere in the presence of a polymer film, and then the metal complex was reduced to produce the Pd nanoparticles. Using this technique, an assembly of metal nanoparticles in block copolymer films [20,21] and a patterning of metal nanoparticles in a polymer thin film by photo- and EB lithography were reported [22,24]. We have also reported on some properties of the Pd nanoparticles thus prepared in a polymer film, as a catalyst for electroless deposition [25] and as a lithography mask for reactive ion etching [23]. The current article discusses the distribution of metal particles incorporated into crystalline polymer films using the one-step dry process, and the effects of their loading on the structures and thermal properties of these films.

2. Experimental section

2.1. Materials

Palladium(II) bis(acetylacetonate), $Pd(acac)_2$, and platinum(II) bis(acetylacetonate), $Pt(acac)_2$, were purchased from Johnson Matthey Materials Technology, and recrystallized in acetone prior to their use. 1,8,9-Trihydroxyanthracene (dithranol), silver trifluoroacetate (AgTFA) and tetrahydrofuran (THF) were purchased from Wako Pure Chem. Ind. Ltd. (Japan) and were used as received. Poly(*tert*-butyl methacrylate) (P*t*BuMA, $M_n = 337{,}000$), atactic polystyrene (aPS, $M_n = 200{,}000$), polyamide 6 (PA6, $M_w = 20{,}000$), and poly(ethylene terephthalate) (PET, $M_w = 18{,}000$) were purchased from Aldrich Chemical Co. (USA), and syndiotactic polystyrene (sPS, $M_n = 250{,}000$) was purchased from Polymer Source Inc. (Canada). A monodispersed aPS (TSK standard, $M_n = 1.04 \times 10^4$, $M_w/M_n = 1.02$) was purchased from Toso Corp. (Japan). Isotactic polypropylene (iPP, $M_n = 224{,}000$, $M_w/M_n = 2.5$) containing no commercial additives was supplied by Chisso Ltd. (Japan). The polymer films with a thickness of 100 μm were prepared by press molding.

2.2. Incorporation of metal nanoparticles into the polymer films

$Pd(acac)_2$ or $Pt(acac)_2$ used as precursor was coated on the upper part of a glass vessel before the loading of a polymer film in order to expose the vapor of the metal complex to the film uniformly. The bottom of a glass vessel with 10 mg of $Pd(acac)_2$ or $Pt(acac)_2$ was heated at 180 °C in an oil bath in vacuo to sublime them, and then, within a few minutes, the vaporized precursors were solidified again on the upper part and were fixed on the glass wall. Next, a polymer film was loaded into the glass vessel. In order to expose the vapor on both sides of the film evenly, the film was fixed in a metal frame with a 1 × 3 cm open window, and was placed perpendicular to the bottom of the vessel as illustrated in Fig. 1. The lower part of the sealed glass vessel including the sample and the metal complex was dipped into an oil bath at 180 °C for 30, 60 or 120 min after nitrogen replacement. In our previous studies, we have confirmed that the vapor of the metal complex could penetrate into a film up to 100 μm in depth [27]. Thus, the exposure from both side of a film can prepare uniform distribution of the metal nanoparticles.

2.3. Instrumental analysis

To study the thermal degradation characteristics of polymer/metal nanocomposites, thermogravimetric analysis (TGA) was employed using a thermal analysis system (TG/DTA 6200, EXTRA 6000 series, Seiko Instruments Inc., Japan). The analysis was carried out at a nitrogen (N_2) flow rate of 200 mL/min to prevent the oxidation of the composites. Film chips with a weight of 3–4 mg were used as sample. Dynamic runs were carried out from room temperature to 600 °C at heating rates of 5, 10, 15 and 20 °C/min, and isothermal runs were carried out at 400 °C for iPP and at 360 °C for sPS in N_2 atmosphere. The Pd nanoparticle contents in polymer films were estimated from ash contents in a sample of about 5 mg by pyrolysis of the films at 800 °C for 1 h in an electric furnace of the TGA apparatus under dry argon atmosphere. The sensitivity of the TGA apparatus is 0.2 μg, and thus the minimum content to be measured is 0.004 wt% of a 5 mg sample. The Pd contents were also estimated from the density of the films measured by a pycnometer (Accupyc-1330, Shimazu Corp., Japan).

Transmission electron microscopy (TEM) was employed with a LEO922 energy-filtering transmission electron microscope (Carl Zeiss Co. Ltd., Germany) at an accelerating

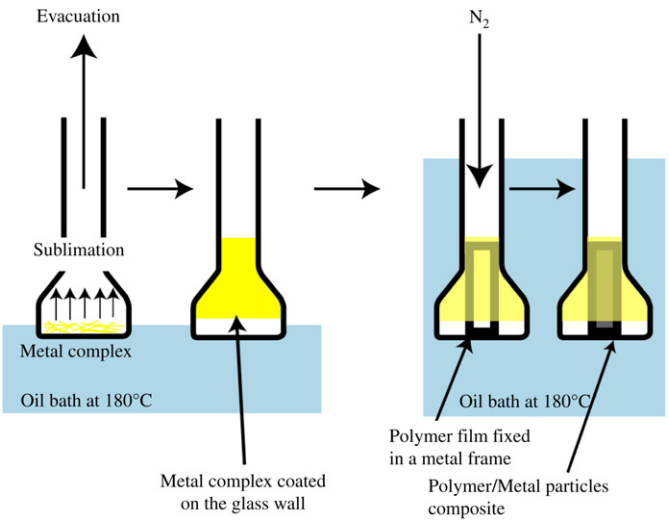

Fig. 1. Illustration representing the scheme of the process for introducing metal nanoparticles into polymer films employed in this study.

voltage of 200 kV. For sPS, thin sections were prepared by cryo-ultramicrotomy at −60 °C after embedding in a light curable resin (D-800, JEOL DATUM, Japan), and then the sections were stained with ruthenium tetroxide (RuO_4) vapor for 10 min. For iPP, the embedded film with a microtomed surface was exposed to RuO_4 vapor overnight, and then it was microtomed at room temperature. The unstained sections of iPP were obtained by cutting the film by cryo-ultramicrotomy at −60 °C. The particle sizes and the size distributions were estimated using image processing software, analySIS® (Soft Imaging System, Germany). The diameters of at least 200 particles in an image were measured and averaged.

A matrix-assisted laser desorption/ionization time-of-flight mass spectrometer (MALDI-TOF MAS, Bruker Daltonics Reflex III, USA) equipped with a pulsed nitrogen laser, of which wavelength and pulse width were 337 nm and 3 ns, respectively, was used for the measurements of molecular weights of polymers. The instrument was operated in reflection mode at a high voltage of 20 kV with positive ions detection. Polymer, 10 mg/mL dithranol in THF (tetrahydrofuran) and 1 mg/mL AgTFA in THF (1 mg/mL) were mixed in a volume ratio of 1:4:1, just before collecting spectrum.

Dynamic mechanical analysis (DMA) was carried out with a Perkin Elmer thermal analysis system at a frequency of 0.5 Hz and a heating rate of 3 °C/min. The sample dimensions for this analysis were $10 \times 2 \times 0.1$ mm.

3. Results and discussion

3.1. Selective incorporation of Pd nanoparticles into semi-crystalline polymers

Fig. 2 shows TEM micrographs of the cross sections of sPS (Fig. 2a and b) and iPP (Fig. 2c and d) films incorporated with Pd nanoparticles prepared by the exposure of $Pd(acac)_2$ vapor for 30 min. The images of unstained specimens are shown in Fig. 2a and c, whereas the images of the specimens stained with RuO_4 are shown in Fig. 2b and d. The particle distributions in the films are independent of the depth from the film surfaces. This suggests that by exposing the vapor of the metal complex on both sides of the films, it can be absorbed and evenly diffused into the inside of the films. In the sPS film, Pd nanoparticles with an average diameter of 6.0 nm and with a standard deviation of 1.5 nm are evenly distributed. While in the iPP film, the Pd nanoparticles are distributed unevenly as they have aggregated to form large domains. As shown in the inset of Fig. 2c, the size of the individual particles in an agglomerated particle is similar to that obtained in the sPS nanocomposite.

As shown in Fig. 2b and d, staining with RuO_4 is helpful in viewing the lamellar morphologies of the crystalline polymers, as it selectively stains the amorphous regions formed by tie molecules jointing the lamellae. The well-distributed Pd

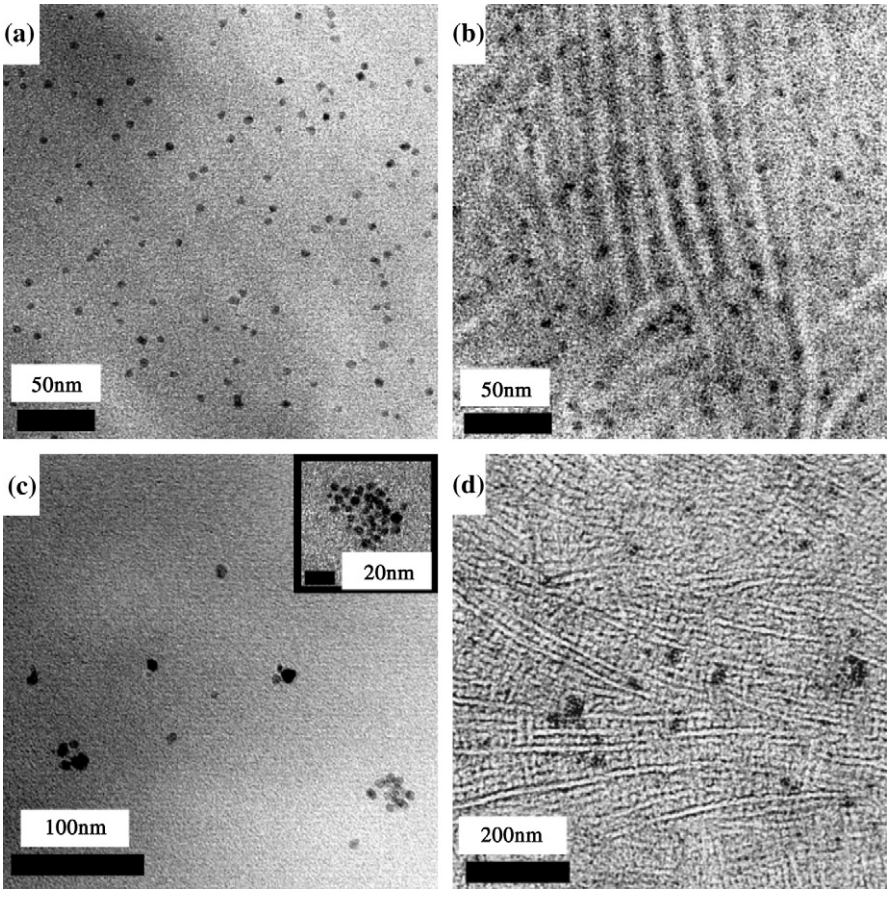

Fig. 2. TEM micrographs of cross sections of sPS/Pd (a and b) and iPP/Pd nanocomposite (c and d) films prepared by the exposure of $Pd(acac)_2$ vapor for 30 min. (a) and (c) are the images of unstained specimens, while (b) and (d) are the images of stained specimens with RuO_4.

nanoparticles are selectively located in the amorphous regions between the lamellae in sPS (Fig. 2b), while the agglomerated Pd particles are located outside of the lamellae in iPP (Fig. 2d). The difference in the location of the Pd nanoparticles in the semi-crystalline polymers is attributed to the difference in the melting temperatures (T_m) of the polymers. The processing temperature of 180 °C is lower than the T_m of sPS (273 °C), and higher than the T_m of iPP (163 °C). Thus, the lamellar structures of sPS are maintained when the $Pd(acac)_2$ vapor is absorbed and reduced to form the Pd nanoparticles. On the other hand, the $Pd(acac)_2$ vapor is absorbed and reduced in iPP in the melt state. It is speculated that during the re-crystallization process of iPP, the macro-Brownian motion of iPP chains and the formation of the lamellae structures exclude the Pd nanoparticles, thus leading to their aggregation.

As reported in our earlier works, the site selectivity of the metal nanoparticles in polymer films could be achieved using nanodomain structures of block copolymer films [20,21]. The metal nanoparticles were selectively produced within the phase having relatively higher reducing power among various components of the films, resulting in either a three-dimensional or a two-dimensional periodical arrangement of metal nanoparticles. On the other hand, the site selectivity of the Pd nanoparticles in the crystalline polymers studied here is achieved owing to the difference between the amorphous and the crystalline structures in the same polymer. It is easier for Pd nanoparticles to form in the amorphous region, as it is softer than the crystal region.

The Pd content in the polymer films was estimated from the residue after the pyrolysis and was plotted against the exposure time of the $Pd(acac)_2$ vapor as in Fig. 3. Those values were the average of four measurements that showed no large scatterings within the same polymers. The measured residue of the composite films is therefore only due to the inorganic components in the films, because we confirmed that the organic polymers give no ash residue after pyrolysis as shown later.

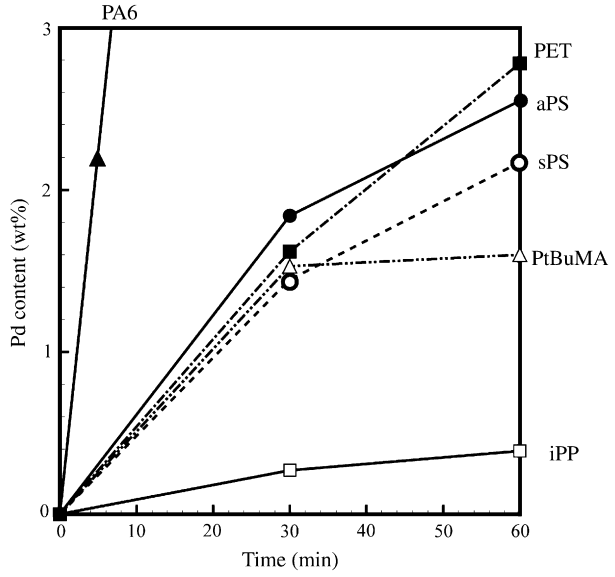

Fig. 3. Plots of Pd contents as a function of the exposure time of $Pd(acac)_2$ vapor in various polymer films.

The contents of Pd nanoparticles in the polymer films varied widely. Especially, PA6 produced Pd nanoparticles at significantly higher contents compared to the other polymers. Exposure of the $Pd(acac)_2$ vapor for 30, 60 and 120 min to the PA6 film produced Pd nanoparticles with the contents of 13, 15 and 23 wt%, respectively. The Pd contents in PA6 were also calculated from the densities of the films, which gave 12, 17 and 23 wt% for the sample exposed to the vapor for 30, 60 and 120 min, respectively.

As illustrated in Fig. 1, the polymer films after the exposure of the $Pd(acac)_2$ vapor turned to be black due to the production of the Pd nanoparticles, while the coated $Pd(acac)_2$ on the vessel remained yellow. This indicates that the polymers themselves work as reducing agents for Pd^{2+} ions. The results shown in Fig. 3 suggest that the structures of polymers have great influence on the efficiency of the production of Pd nanoparticles. The yield of Pd nanoparticles is assumed to depend on the reducing power of the polymers against the metal complex and also on the rate of diffusion of the metal complex into the polymer films. The highest yield obtained by PA6 is owing to the amino end group of PA6 that works as a strong reducing agent. iPP, on the other hand, showed the lowest yield among the polymers evaluated, which might be attributed to the non-polar chemical structure. Polarity of the chemical structures, however, does not lead to high yield of the metal nanoparticles. As was reported in our previous works, poly(methyl methacrylate), (PMMA), has uniquely poor reducing power although it has carbonyl polar group in the side chain [21,22]. We speculate that the Pd^{2+} ions can be stabilized through the coordination with the carbonyl group in the PMMA side chain. Thus, P*t*BuMA gave a little lower yield than polystyrenes and PET. It is noteworthy that the semi-crystalline polymers with higher melting temperatures than the processing temperature (sPS, PA6 and PET) can produce the Pd nanoparticles at the levels similar to the amorphous polymers (aPS and P*t*BuMA). This means that the $Pd(acac)_2$ vapor can be absorbed and diffused into the crystal phases in polymers. The Pd contents in sPS are slightly lower than in aPS, which suggests a lower rate of diffusion of the $Pd(acac)_2$ vapor due to the existence of the hard crystalline phase.

Fig. 4 shows TEM micrographs of PA6 and PET exposed to $Pd(acac)_2$ vapor for 30 min. Both polymers show uniform distributions of Pd nanoparticles in the films. The average diameters of the Pd nanoparticles are 3.4 and 3.7 nm with standard deviations of 0.9 and 1.4 nm in PA6 and PET, respectively, which are smaller than those in sPS. The particle size is determined by the competition between nucleation and growth of the particles. In a system with strong reducing power, nucleation is faster than the growth of particles, resulting in small particle size. It is assumed that PA6 and PET can more effectively produce nucleating sites than polystyrenes, indicating that those polymers have stronger reducing power than polystyrenes. The T_ms of PA6 and PET are 220 and 265 °C, respectively, which are higher than the processing temperature. Therefore, the Pd nanoparticles are produced in the polymer films while maintaining the crystalline morphologies similar to that in the sPS.

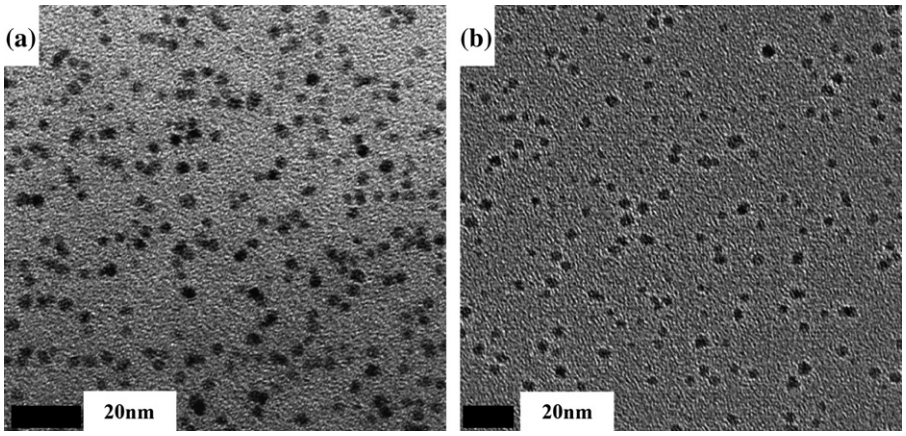

Fig. 4. TEM micrographs of cross sections of (a) PA6 and (b) PET films exposed to $Pd(acac)_2$ vapor for 30 min.

3.2. Effect of the process on chemical structures of the polymers

To study how the molecular structures of the polymers are changed during the loading process of the Pd nanoparticles into the polymers, MALDI-TOF MAS and FTIR analyses were carried out. Fig. 5a shows the MALDI-TOF MAS spectra of a monodispersed aPS with M_n of 1.02×10^4 before (upper spectrum) and after (bottom spectrum) the exposure of the $Pd(acac)_2$ vapor for 30 min. No major changes in the molecular weight distribution were detected in the two spectra, indicating that the metal loading process did not cause any degradation or crosslinking of the polymer. These results were corroborated with FTIR analysis in case of iPP and PA6 films. Fig. 5b and c shows the FTIR spectra before and after the metal loading process in iPP and PA6 films, respectively. The spectra presented with solid and dotted lines correspond to those before and after the process, respectively. No new peaks or shifts in the peaks are observed after the loading of the Pd nanoparticles. These results indicate that the Pd nanoparticles can be introduced into polymer films without causing any significant changes in the polymer structures.

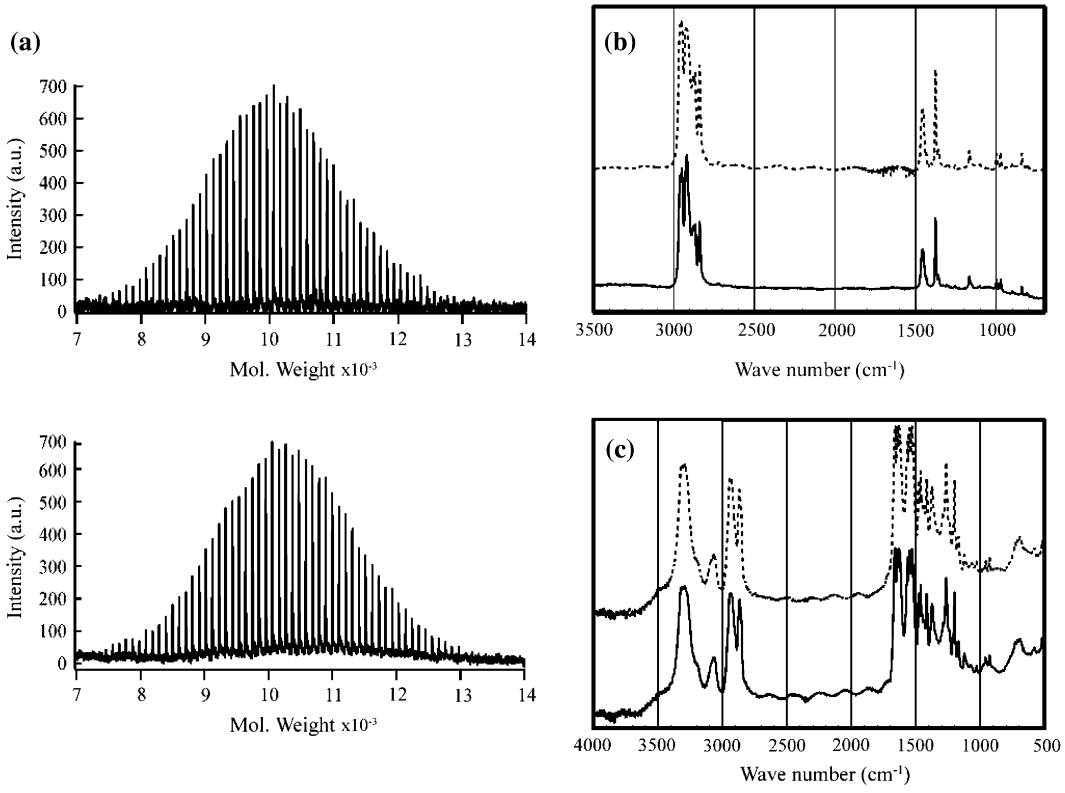

Fig. 5. (a) MALDI-TOF MAS spectra of a neat aPS ($M_n = 1.04 \times 10^4$) (top) and the sPS nanocomposite (bottom) prepared by the exposure of $Pd(acac)_2$ vapor for 30 min. (b) and (c) FTIR spectra of iPP and PA6 nanocomposite films, respectively. Spectra shown by solid lines correspond to the neat polymers and those shown by dotted lines correspond to the nanocomposites.

The thermal decomposition temperature (T_d) of the bulk $Pd(acac)_2$ in nitrogen is 220 °C [7]. Thus, the polymers can decrease the T_d of $Pd(acac)_2$ to 180 °C or lower without any changes in their molecular structures. $Pd(acac)_2$ introduced into polymer films in different ways could also be thermally decomposed and reduced to form Pd nanoparticles. $Pd(acac)_2$ can be dissolved in a aPS film up to 10 wt% by casting from a chloroform solution [27]. Then, $Pd(acac)_2$ is decomposed to form Pd nanoparticles by thermal treatment at 180 °C or lower. The achieved Pd contents by this method, however, were quite lower than by our method because $Pd(acac)_2$ dissolved in the polymer film was evaporated during the thermal treatment. Supercritical CO_2 is also effective to introduce $Pd(acac)_2$ into polymer films, and Pd nanoparticles could be distributed into polyimide films by thermal treatment at a lower temperature of the T_d of $Pd(acac)_2$ [11]. These facts indicate that polymers have catalytic ability to decompose the metal complex, although we do not know the precise mechanism of the thermal decomposition of $Pd(acac)_2$ in polymers. However, it has been reported that similar to the polymers, organic solvents can also reduce the T_d of metal complexes [28]. The organic solvents are thought to stabilize a transition state of metal species and lower the activation energy for thermal decomposition by the coordination. Further, the byproducts of the decomposition of $Pd(acac)_2$ were not detected in the polymer films, which indicated that they were evaporated during the process.

Fig. 6 shows the storage modulus of the sPS and the PA6 nanocomposite films with various Pd contents as a function of temperature, measured by DMA. The incorporation of the Pd nanoparticles did not lead to deterioration of the thermomechanical behavior. Moreover, the storage modulus of PA6 can be enhanced due to the high loading of the Pd nanoparticles. These results further confirm that the metal loading process does not cause any degradation of the host polymers. However, the incorporation of Pd nanoparticle lowers the glass transition temperature estimated from the onset at which the storage modulus is decreased, suggesting that the crystalline structures and/or crystallinity might be changed by the absorption of $Pd(acac)_2$.

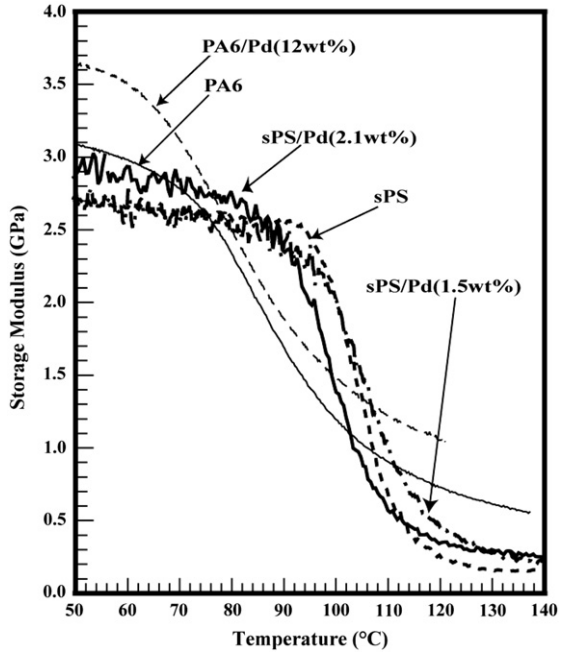

Fig. 6. Temperature dependences of the storage modulus of PA6 and sPS nanocomposite films with various Pd contents measured by DMA.

3.3. Effect of metal nanoparticles on thermal degradation behavior of polymers

The thermal stability of the polymer films incorporated with the Pd nanoparticles was investigated by thermogravimetric analysis (TGA). Fig. 7a and b shows the TGA curves of the dynamic runs at the heating rate of 10 °C/min in a nitrogen atmosphere for sPS and for iPP incorporated with various amounts of the Pd nanoparticles, respectively. It is clear that the addition of the Pd nanoparticles shifts the TGA curves to higher temperatures. In the case of pure sPS, there is almost no weight loss before 360 °C, but the degradation rate becomes very quick beyond that temperature, and almost all polymer chains are degraded abruptly between 360 and 450 °C. The exposure of $Pd(acac)_2$ vapor for 30 min to the sPS film gave 1.5 wt% of the Pd nanoparticles, which is equal to 0.12 vol% (density of Pd is 12.02 g/cm^3). Incorporation of this small amount of the Pd nanoparticles into sPS remarkably improves the thermal stability because it increases the temperature at which the degradation begins by about 50 °C and most of the degradation occurs at a higher temperature range of between 410 and 450 °C. Higher loading of the Pd nanoparticles (2.1 wt%) does not lead to any further improvement of the thermal stability. In the case of iPP, where the Pd contents that could be loaded were much lower than those in sPS, the thermal stability was also improved satisfactorily. Isothermal TGA curves for sPS and for iPP are also shown in Fig. 7c and d, respectively. The annealing temperatures were 360 °C for the sPS films, and 400 °C for the iPP films. These figures clearly show that the addition of Pd nanoparticles significantly retards the thermal degradation of the polymers, as the time (T_τ) taken for 50 wt% of the polymer to degrade is about two times longer than those for the pure sPS and iPP.

It is amazing that such a small amount of the Pd nanoparticles can improve the thermal stability of the polymers remarkably. We have confirmed that the Pd nanoparticles also improve the thermal stabilities of aPS and P*t*BuMA, and it has been reported that the thermal decomposition of PMMA was also retarded by the incorporation of Pd nanoparticles [19]. Moreover, the use of $Pt(acac)_2$ as an alternative to $Pd(acac)_2$ leads to incorporation of Pt nanoparticles into a sPS polymer film, and its thermal stability is also improved in a same manner. The exposure of $Pt(acac)_2$ vapor for 30 min gives 1.5 wt% of Pt content in sPS, and increases the onset of the thermal degradation in the dynamic run at 10 °C/min by 55 °C.

On the other hand, the Pd nanoparticles affect the thermal stability of PA6 and PET negatively as shown in Fig. 8a and b,

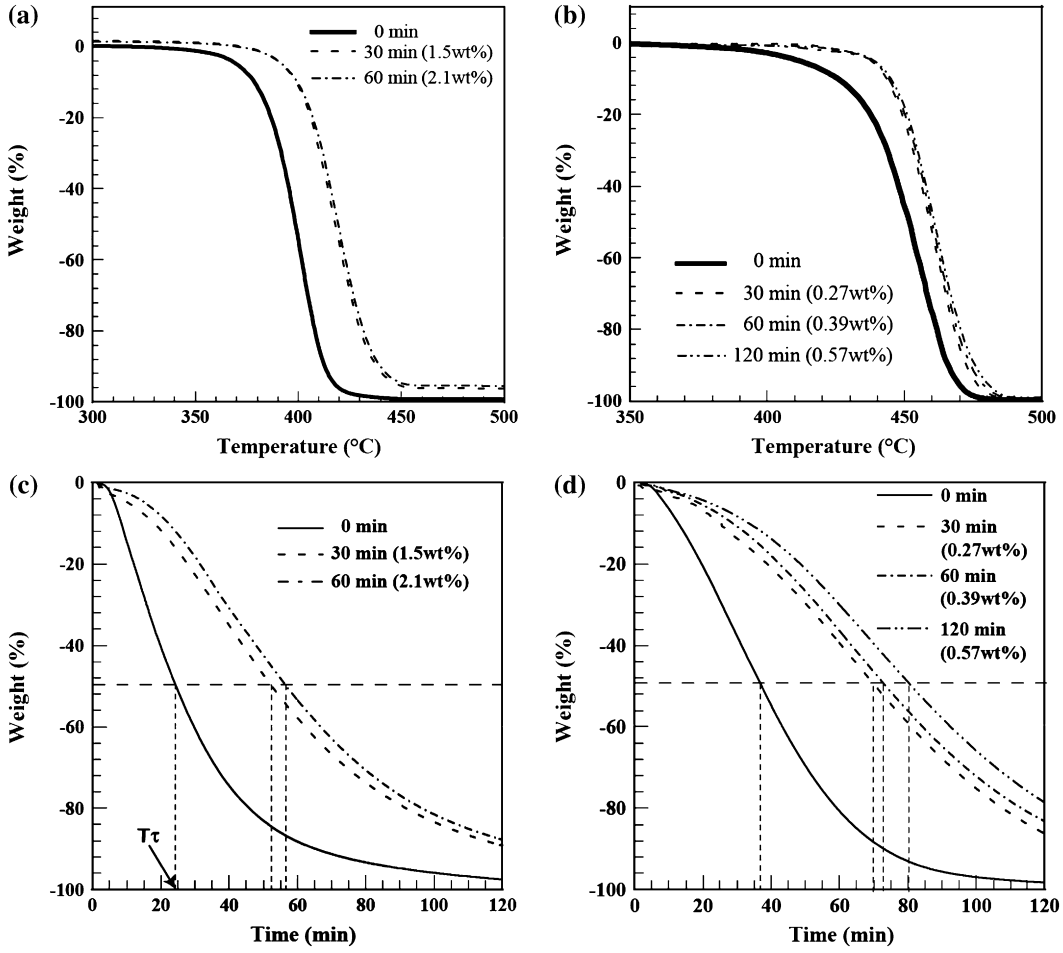

Fig. 7. (a) and (b) TGA curves of dynamic runs at 10 °C/min under nitrogen for sPS and iPP nanocomposite films, respectively. (c) and (d) TGA curves of isothermal runs under nitrogen for sPS nanocomposite films at 360 °C and for iPP nanocomposite films at 400 °C, respectively.

respectively. In both the polymers, the incorporation of the Pd nanoparticles shifts the TGA curves to lower temperatures. Therefore, it is clear that the Pd nanoparticles accelerate the thermal degradation for PA6 and PET.

3.4. Kinetic analysis of thermal degradation

In order to understand the mechanism of the effect of the Pd nanoparticles on the thermal degradation behavior, the results

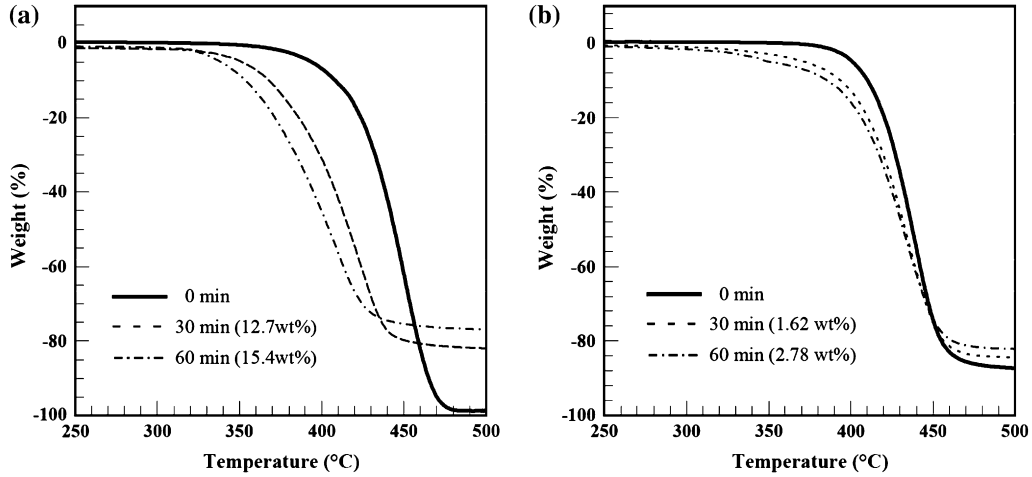

Fig. 8. TGA curves of dynamic runs at 10 °C/min under nitrogen for (a) PA6 and (b) PET nanocomposite films with various Pd content.

of TGA measurements at different heating rates were subjected to thermal degradation kinetics studies. Since the polymer structures are maintained through the incorporation process of the Pd nanoparticles, we could estimate the thermal degradation activation energy (E_d) and frequency factor (A) of the polymers. Thus, we could discuss the chemical and the physical effects of the Pd nanoparticle on the thermal degradation separately.

For many kinetic processes, a rate of reaction may be expressed as a product of the rate constant, k, and composition dependent term, $f(\alpha)$:

$$r = \frac{d\alpha}{dt} = kf(\alpha) \tag{1}$$

where α is the conversion (=weight of the polymer volatilized/initial weight of the polymer) and r is the rate of change of conversion per unit time (t). The rate constant is a temperature dependent term, which is assumed to obey the usual Arrhenius relationship:

$$k = A\exp\left(\frac{-E_d}{RT}\right) \tag{2}$$

where E_d is the degradation activation energy, A is the pre-exponential factor, T is the absolute temperature, and R is the gas constant (8.314 J/mol K). The term $f(\alpha)$ is assumed to follow a simple nth order relationship:

$$f(\alpha) = (1-\alpha)^n \tag{3}$$

Combining Eqs. (1)–(3) leads to the following expression:

$$\frac{d\alpha}{dt} = A(1-\alpha)^n \exp\left(\frac{-E_d}{RT}\right) \tag{4}$$

We estimated the kinetic parameters by applying two separate methods to the TGA and the corresponding differential thermogravimetric (DTG) data, taken at different heating rates of 5, 10, 15 and 20 °C/min.

Kissinger method derives a useful expression from Eq. (4) that allows the calculation of E_d from the temperature, T_p, at the maximum of DTG curves, where the maximum weight loss rate appears, obtained from runs at a number of heating rates [28,29].

$$\frac{d\left[\ln\left(\beta/T_p^2\right)\right]}{d\left(1/T_p\right)} = -\frac{E_d}{R} \tag{5}$$

where β is the heating rate. The E_d can be calculated from the slope of the straight line in the plot of $-\ln(\beta/T_p^2)$ versus $1/T_p$.

Friedman's method, on the other hand, derives the following equation from Eq. (4) [30]:

$$\ln\beta\left(\frac{d\alpha}{dT}\right) = \ln A + n\ln f(\alpha) - \frac{E_d}{RT} \tag{6}$$

The reaction rate, $d\alpha/dt$, is plotted against $1/T$ at an equal conversion, where T values at a constant α are taken from TGA curves at different scanning rates. Therefore, if the kinetics does not change with the conversion, one should observe a family of parallel lines having $-E_d/R$ as slope. In addition, the reaction order, n and the frequency factor, A can be obtained from the plots of E_d/RT_0 versus $\ln(1-\alpha)$, where T_0 is the temperature at which $\ln(\beta d\alpha/dT)$ is equal to zero.

Fig. 9 shows the plots of the calculated values of $-\ln(\beta/T_p^2)$ versus $1/T_p$ obtained by applying Kissinger method. The linear relationship between $-\ln(\beta/T_p^2)$ and $1/T_p$ was obtained in all the neat polymers and in the corresponding nanocomposites prepared by the exposure of the $Pd(acac)_2$ vapor for 30 min. The activation energies were calculated from the slopes by Eq. (1) and are shown in Table 1.

Fig. 10a shows typical plots of the calculated values of $\ln(\beta d\alpha/dT)$ versus $1/T_p$ obtained by applying the Friedman method to the sPS nanocomposite with the Pd content of 1.5 wt%. A linear relationship between the two parameters was obtained with all the evaluated conversion points ($\alpha = 0.2$–0.8). Next, E_ds were calculated for each α, and the averages and the standard deviations are presented in Table 1. In order to obtain the reaction order, n, and the frequency factor, A, a second plot (Fig. 10b) was created. This graph includes the results of the neat sPS and the sPS nanocomposite with 1.5 wt% Pd content. In both the cases, the plots exhibit good linear relationships and thus n could be calculated from the slopes and A could be estimated from the intercepts.

All the kinetic parameters calculated by the two methods are listed in Table 1. The activation energies computed by the two methods are similar, and they are in good agreement with those previously reported for neat polymers [31–33]. For sPS and iPP, there are no significant differences in the E_ds of the neat polymers and the corresponding composite materials, while the incorporation of the Pd nanoparticles results in about 20% reduction in the activation energy of

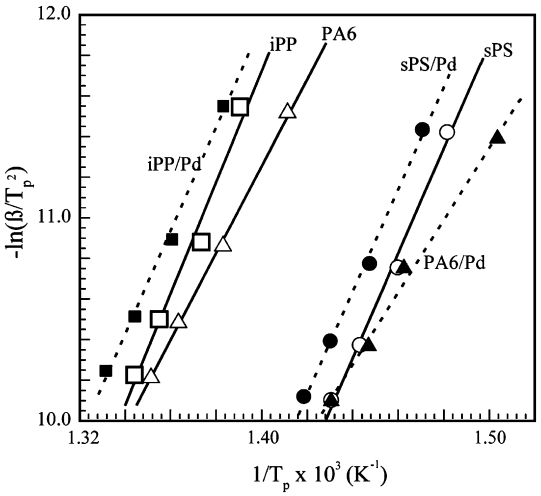

Fig. 9. Application of Kissinger method to the DTA data for PA6 and iPP neat polymers and for the corresponding nanocomposites prepared by the exposure of $Pd(acac)_2$ vapor for 30 min.

Table 1
Kinetic parameters calculated from TGA and DTA curves

Sample	Method	E_d (kJ/mol^{-1})	A (min^{-1})	n
sPS	Friedman	223 ± 7.6	3.8×10^{16}	0.8
	Kissinger	215		
sPS/Pd (1.5 wt%)	Friedman	220 ± 3.7	1.1×10^{16}	0.9
	Kissinger	209		
iPP	Friedman	229 ± 13.1	6.5×10^{15}	0.5
	Kissinger	228		
iPP/Pd (0.27 wt%)	Friedman	226 ± 11.0	3.4×10^{15}	0.5
	Kissinger	211		
PA6	Friedman	184 ± 5.2	7.5×10^{12}	0.6
	Kissinger	178		
PA6/Pd (12.7 wt%)	Friedman	134 ± 14.3	6.0×10^{9}	0.9
	Kissinger	146		

PA6. Pre-exponential factor, A, on the other hand, tends to decrease with the incorporation of the Pd nanoparticles into all the three polymers, and it decreases with increase in Pd content loaded into the polymers.

The enhancement of the thermal stability by the Pd nanoparticles in sPS and iPP could mainly be attributed to the decrease in the pre-exponential factor. This decrease indicates that the collision frequency of the polymer chains largely decreases, thereby suggesting that the mobility of the polymer chains is greatly suppressed by the Pd nanoparticles. It is well known that the thermal degradation of a polymer begins with the generation of free radicals, which transfer to the adjacent chains via intermolecular and intramolecular chain reactions, followed by a termination step [34]. Thus, it is indicated that the Pd nanoparticles have an ability to greatly suppress these chain transfer reactions. On the other hand, thermal degradation of PA6 is accelerated due to the reduction in the activation energy by the Pd nanoparticles, the effect of which is greater than the decrease in the pre-exponential factor. This suggests that the Pd nanoparticles have a catalytic role in the degradation of PA6.

4. Conclusions

The Pd nanoparticles were incorporated into the polymer films via a dry route using a metal complex without the aid of any solvents or reducing agents. Although the mechanism of the reduction and formation of the nanoparticles in the polymer films remain unclear, it was shown that the polymers maintained their molecular structures throughout the process. The Pd nanoparticles could be successfully incorporated into the crystalline polymers having melting temperatures higher than the processing temperature (180 °C). In these cases, the Pd nanoparticles were selectively located in the amorphous regions between the lamellae. Therefore, this method enables us to introduce metal nanoparticles into polymer films with poor solubility and high melting temperatures.

We found that even an extremely small amount of Pd nanoparticles can significantly enhance the thermal stability of some polymers, while being harmful to some other polymers. The kinetic studies of the TGA analysis results suggest that the Pd nanoparticles reduced the frequency factor of the polymers, thus suppressing the mobility of the polymer chains, and thereby suppressing the degradation reactions of sPS and iPP. On the other hand, the addition of Pd nanoparticles led to a reduction in activation energy, and thus had a catalytic role in the degradation reactions of PA6. Therefore, the Pd nanoparticles have both physical and chemical effects on the thermal degradation of polymers. Much more types of polymers have to be evaluated in order to find a rule to classify polymers into two groups.

The metal nanoparticles may have possible applications in melt processing of polymers due to their thermal stabilization effects. Conventionally, hindered phenol derivatives have mainly been used for the thermal stabilizers of polymers. However, these organic compounds cause deterioration in the mechanical properties of the resultant products. The selective incorporation of metal nanoparticles into amorphous regions

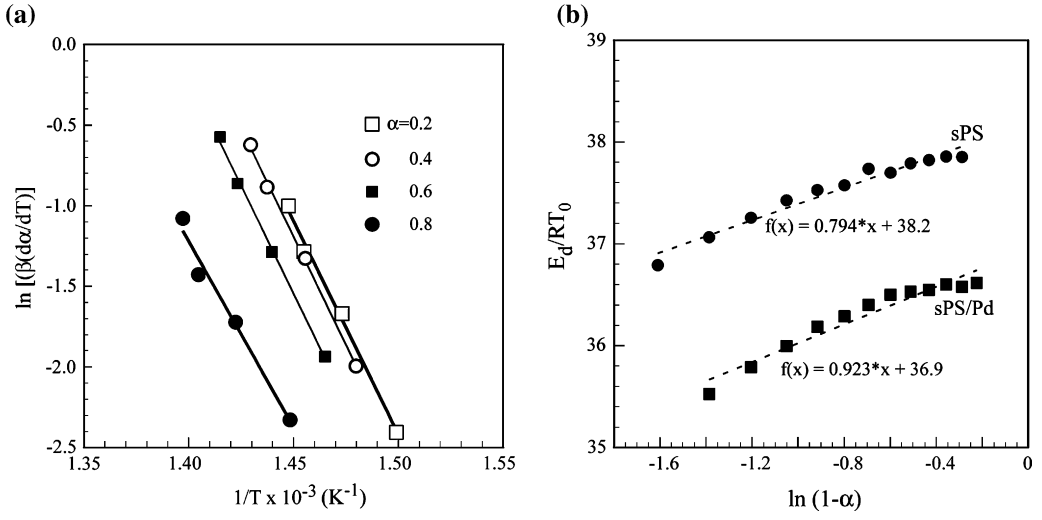

Fig. 10. Application of Friedman method to the DTG data for neat sPS and the sPS nanocomposite film with Pd content of 1.5 wt%. (a) Plot for obtaining of thermal degradation activation energies at different conversions (α). (b) Plots for obtaining of frequency factors and reaction orders.

in crystalline polymers may allow us to produce materials that exhibit unique mechanical and thermal properties. We are now investigating the influence of the metal nanoparticles on the properties of crystalline polymers.

Acknowledgement

J.Y. Lee thanks Japan Society for the Promotion of Science (JSPS) for the post-doctoral fellowship.

References

[1] Demir MM, Gulgun MA, Menceloglu YZ, Erman B, Abramchuk SS, Makhaeva EE, et al. Macromolecules 2004;37:1787–92.
[2] dos Santos Jr DS, Goulet PJG, Pieczonka NPW, Oliveira Jr ON, Aroca RF. Langmuir 2004;20:10273–7.
[3] Porel S, Singh S, Harcha SS, Rao DN, Radhakrishnan TP. Chem Mater 2005;17:9–12.
[4] Delamarche E, Geissler M, Vichiconti J, Graham WS, Andry PA, Flake JC, et al. Langmuir 2003;19:5923–35.
[5] Lu C, Guan C, Liu Y, Cheng Y, Yang B. Chem Mater 2005;17:2448–54.
[6] Haes AJ, Zou S, Schatz GC, Van Duyne RP. J Phys Chem B 2004;108: 6961–8.
[7] Nakao Y. J Colloid Interface Sci 1995;171:386–91.
[8] Mibhele ZH, Salemane MG, van Sittert CGCE, Nedeljković JM, Djoković V, Luyt AS. Chem Mater 2003;15:5019–24.
[9] Klabunde KJ, Habdas J, Cardenas TG. Chem Mater 1989;1:481–3.
[10] Boyes SG, Akgun B, Brittain WJ, Foster MD. Macromolecules 2003;36: 9539–48.
[11] Yoda S, Hasegawa A, Suda H, Uchimaru Y, Haraya K, Tsuji T, et al. Chem Mater 2004;16:2363–8.
[12] Zhong CJ, Maye MM, Luo J, Han L, Kariuki N. In: Rotello V, editor. Nanoparticles: building blocks for nanotechnology. New York: Kluwer Academic/Plenum Publishers; 2004. p. 113–43.
[13] Xu Y, Sun HB, Ye JY, Matsuo S, Misawa H. J Opt Soc Am B 2001;18: 1084–91.
[14] Thurn-Albrecht T, Schotter J, Kästle GA, Emley N, Shibauchi T, Krusin-Elbaum L, et al. Science 2000;290:2126–9.
[15] Chou SY, Wie MS, Krauss PR, Fischer PB. J Appl Phys 1994;76:6673–5.
[16] Baranauskas III VV, Zalich MA, Saunders M, St. Pierre TG, Riffle JS. Chem Mater 2005;17:5246–54.
[17] Delamarche E, Vichiconti J, Hall SA, Geissler M, Graham WS, Michel B, et al. Langmuir 2003;19:6567–9.
[18] Luigi N, Carotenuto G, editors. Metal–polymer nanocomposites. Hoboken, New Jersey: John Wiley & Sons; 2005.
[19] Aymonier C, Bortzmeyer D, Thomann R, Mülhaupt R. Chem Mater 2003;15:4874–8.
[20] Horiuchi S, Sarwar MI, Nakao Y. Adv Mater 2000;12:1507–11.
[21] Horiuchi S, Fujita T, Hayakawa T, Nakao Y. Langmuir 2003;19: 2963–73.
[22] Horiuchi S, Fujita T, Hayakawa T, Nakao Y. Adv Mater 2003;15:1449–52.
[23] Yin D, Horiuchi S, Masuoka T. Chem Mater 2005;17:463–9.
[24] Yin D, Horiuchi S, Morita M, Takahara A. Langmuir 2005;21:9352–8.
[25] Lee JY, Yin D, Horiuchi S. Chem Mater 2005;17:5498–503.
[26] Horiuchi S, Fujita T, Hayakawa T, Nakao Y. Kobunshi Ronbunshu 2002; 59:571–7.
[27] Chiba A, Hashimoto T. Polym Prep Jpn 2004;53:3678–9.
[28] Esumi K, Tano T, Meguro K. Langmuir 1989;5:268–70.
[29] Kissinger HE. Anal Chem 1957;29:1702–6.
[30] Lee JY, Shim MJ, Kim SW. J Appl Polym Sci 2001;81:479–85.
[31] Ravanetti GP, Zini M. Thermochim Acta 1992;207:53–64.
[32] Grassie N, Scotney A. In: Brandrup J, Immergut EH, editors. Polymer handbook. 2nd ed. New York: John Wiley & Sons; 1975. p. II469–79.
[33] Chan JH, Balke ST. Polym Degrad Stab 1997;57:135–49.
[34] Schnabel W. Polymer degradation: principles and practical applications. Munich: Carl Hanser Verlag; 1982 [chapter 2].